Environmental Science & Technology

Article

pubs.acs.org/est

Intraparticle Reduction of Arsenite (As(III)) by Nanoscale Zerovalent Iron (nZVI) Investigated with In Situ X-ray Absorption Spectroscopy

Weile Yan,[†,∥] Relja Vasic,[‡] Anatoly I. Frenkel,*[,‡] and Bruce E. Koel*[,§]

[†]Department of Civil and Environmental Engineering, Lehigh University, Bethlehem, Pennsylvania 18015, United States
[‡]Department of Physics, Yeshiva University, 245 Lexington Avenue, New York City, New York 10016, United States
[§]Department of Chemical and Biological Engineering, Princeton University, Princeton, New Jersey 08544, United States

Supporting Information

ABSTRACT: While a high efficiency of contaminant removal by nanoscale zerovalent iron (nZVI) has often been reported for several contaminants of great concern, including aqueous arsenic species, the transformations and translocation of contaminants at and within the nanoparticles are not clearly understood. By analysis using in situ time-dependent X-ray absorption spectroscopy (XAS) of the arsenic core level for nZVI in anoxic As(III) solutions, we have observed that As(III) species underwent two stages of transformation upon adsorption at the nZVI surface. The first stage corresponds to breaking of As−O bonds at the particle surface, and the second stage involves further reduction and diffusion of arsenic across the thin oxide layer enclosing the nanoparticles, which results in arsenic forming an intermetallic phase with the Fe(0) core. Extended X-ray absorption fine-structure (EXAFS) data from experiments conducted at different iron/arsenic ratios indicate that the reduced arsenic species tend to be enriched at the surface of the Fe(0) core region and had limited mobility into the interior of the metal core within the experimental time frame (up to 22 h). Therefore, there was an accumulation of partially reduced arsenic at the Fe(0)/oxide interface when a relatively large arsenic content was present in the solid phase. These results illuminate the role of intraparticle diffusion and reduction in affecting the chemical state and spatial distribution of arsenic in nZVI materials.

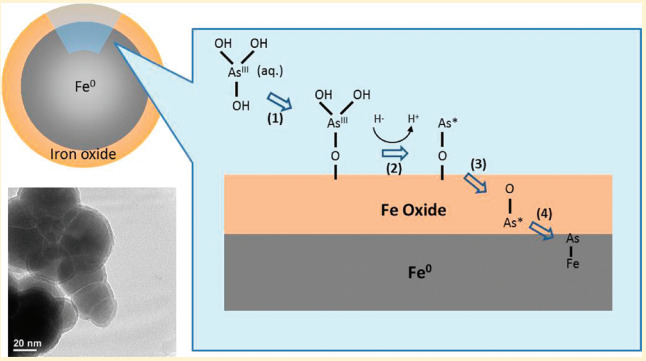

INTRODUCTION

The occurrence of arsenic in groundwater at elevated concentrations across diverse geographical regions is a public health issue of great concern, particularly in semiarid or arid areas and regions with contaminated surface waters, where groundwater is an important source of drinking water.[1−3] Arsenic is present in many naturally occurring minerals, including iron oxides and sulfide-containing minerals, in oxidation states ranging from −3 to +5.[1,2] The dissolved forms of arsenic in water are predominantly the trivalent arsenite (As(III)) and pentavalent arsenate (As(V)) oxyanions. As(V) is the prevalent form in aerobic water, while As(III) is a significant species in subsurface environments including groundwater and aquifer sediments.[2,3] Redox transformations between As(III) and As(V) in the natural environment are considered to be closely tied to the redox cycling of iron and sulfur species via both biotic and abiotic pathways.[4−6] Both forms of arsenic have strong affinity for iron oxide surfaces under circumneutral pH.[7,8] The molecular-level structures of inner-sphere complexes formed between arsenic and a variety of iron oxide surfaces have been elucidated using vibrational and X-ray absorption spectroscopic techniques.[9−12] Their strong interactions have led to the development of many iron oxide-amended sorbent materials suitable for aqueous arsenic removal in small-scale, household-based treatment units, which are attractive alternatives to centralized water treatment facilities.[13,14]

Recent studies demonstrate that zerovalent iron (ZVI), in particular nanoscale zerovalent iron (nZVI), can retain a high level of As(III) and As(V) under laboratory and field conditions.[15−20] Effective arsenic removal is primarily attributed to the adsorption of arsenic onto the passivating oxide layer of ZVI materials[15,18] or coprecipitation with dissolved iron under high arsenic loadings.[21,22] On-going corrosion of ZVI in water supplies a continuous source of surface sites for arsenic adsorption, which is considered a major advantage of ZVI technology compared to conventional treatment using iron oxides.[16,19,20] Although changes in arsenic valence state have been observed during ZVI treatment, the reaction mechanisms and the chemical forms in which arsenic is arrested are not clearly understood. Recent studies reported that As(III) can be

Special Issue: Transformations of Nanoparticles in the Environment

Received: November 7, 2011
Revised: January 27, 2012
Accepted: February 1, 2012
Published: February 1, 2012

oxidized by reactive oxygen species generated from Fe(0) corrosion in aerated water[19,23] or in the presence of Fe(II) and goethite surfaces in anoxic conditions.[24] While As(III) reduction has been observed with nZVI in anoxic conditions,[25,26] it was not detected in systems using bulk-scale ZVI powders.[15,16] Since both the oxidation and reduction of arsenic are considered to be surface-mediated processes, direct spectroscopic analysis of the solid phase has provided insights into arsenic speciation at the surface of iron media. Using X-ray photoelectron spectroscopy (XPS), both As(III) oxidation and reduction were observed at nZVI particle surfaces.[25] Furthermore, using a multiline analysis of the XPS data, stratified distributions of different arsenic species in the nanoparticles were resolved.[26] Oxidized species (As(V)) was observed to be predominantly at the outer surface of the oxide shell, while reduced species were enriched in a subsurface layer close to the Fe(0) core. In principle, the reduced arsenic may segregate as a separate phase or interact with Fe(0) to form iron−arsenic solid solutions or iron arsenide minerals such as loellingite.[27−29] Identifying the nature of the embedded arsenic requires techniques that are capable of probing the core or bulk of the nanoparticles and generating data related to the local bonding environment of arsenic. Although XPS is a powerful tool to investigate the chemical state and near-surface depth distribution of arsenic in nZVI, it is commonly conducted in ultrahigh vacuum and has a probing depth limited to ∼10 nm beneath the sample surface. Additionally, absolute quantification of species distributed inhomogeneously throughout the sampling depth is complicated by the fact that the photoelectrons are attenuated to different extents with depth.[30] To overcome these limitations, synchrotron-based X-ray absorption spectroscopic analysis, i.e., X-ray absorption near-edge structure (XANES) and extended X-ray absorption fine structure (EXAFS), was applied in situ using a reaction cell containing nZVI and aqueous As(III) solutions. This analysis enabled us to examine the dynamic changes in the arsenic chemical state over time in the reaction medium and to investigate in detail the bonding environments of arsenic at and within the nanoparticles under varying conditions. Results from this present study have direct implications for the potential use of nZVI for in situ groundwater remediation. These results may also find relevance in natural systems where arsenic may be present in multiple states in different forms of coexisting iron-bearing solids.

EXPERIMENTAL METHODS

Materials. Iron nanoparticles (nZVI) were synthesized from ferric chloride using borohydride reduction as reported previously.[31,32] The median size of the as-synthesized nanoparticles was approximately 60 nm as measured by transmission electron microscopy (TEM) and acoustic spectrometry.[32] The As(III) stock solution was prepared from sodium arsenite ($NaAsO_2$, Fluka) in deoxygenated deionized water.

In Situ Reaction Samples. *In situ* XAS studies of reactions between As(III) and nZVI were performed in a customized reaction cell shown schematically in Figure 1. Details about the construction of the cell are available in the Supporting Information. Solutions containing As(III) and nZVI were injected into the cell through two screw-sealed bore openings on the top of the cell. To prevent the nanoparticles from settling out at the bottom of the cell during X-ray scans, the cell was filled with a small amount of quartz wool. Anchoring of nanoparticles on the quartz wool gives a characteristic black

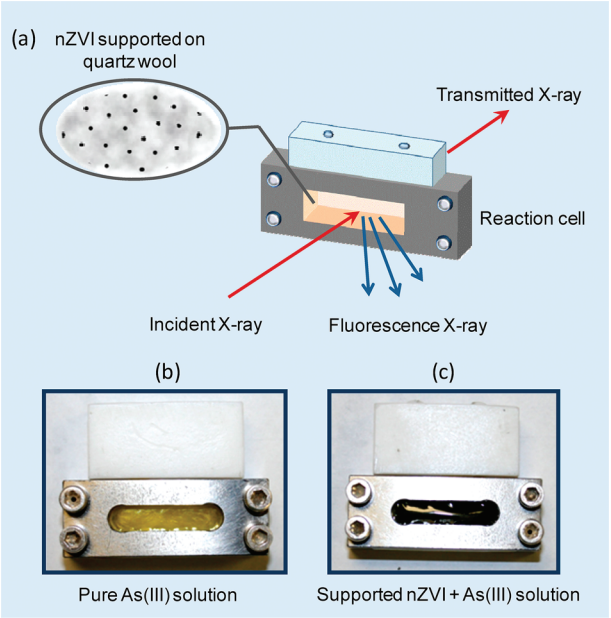

Figure 1. (a) Schematic of the experimental setup for in situ XAS studies. Photographs of (b) a reaction cell filled with pure As(III) solution and (c) supported nZVI in As(III) solution.

color as shown by the photographs in Figure 1. The constant absorption edge step that was observed over the duration of the experiment attests to the lack of detectable change in the sample content probed by the X-ray beam as a function of time. All experiments and cell preparations were performed in anoxic conditions in a N_2 glovebox. A typical experiment was started by mixing an appropriate amount of nZVI (2−5 g/L) into an aqueous As(III) solution (1.33 mM) in a glass vial. A small aliquot (∼1.5 mL) of the mixture was then loaded into the cell, and the cell was packed in an airtight Ziploc bag and transferred immediately into the X-ray analysis chamber for time-resolved measurements. The mixture in the glass vial was allowed to react for up to 22 h before the final products were analyzed.

X-ray Absorption Analysis. In situ X-ray absorption measurements were performed at beamline X18B of the National Synchrotron Light Source (NSLS) at Brookhaven National Laboratory. The synchrotron ring was operated at 2.8 GeV and at currents between 150 and 300 mA. The reaction cell was mounted onto a sample holder and placed in a N_2-filled chamber. Scans were performed at room temperature in fluorescence mode at the arsenic K-edge (over the energy range of 11717−13397 eV) and iron K-edge (6962−8352 eV). The Si(111) double-crystal monochromator was detuned by 20% at the arsenic K-edge and 30% at the iron K-edge, respectively. Reagent grade sodium arsenate ($Na_2HAsO_4{\cdot}7H_2O$, Fluka) powder was used as an internal reference for the arsenic K-edge measurements. For the iron K-edge, spectra were calibrated with an iron foil reference sample.

Except for the pure As(III) solution, which was measured with an argon-filled five-grid Lytle detector, arsenic signals in samples containing nZVI were measured with a four-element silicon-drift Vortex detector because of its improved signal-to-noise level. For the Lytle detector, a germanium filter and Soller slits were used to reduce Compton and elastic scattering from the samples. XANES spectra were collected at a step size of 0.5 eV near the edge with an integration time of 0.5 s to allow real-time monitoring of arsenic speciation at ∼5 min intervals.

dx.doi.org/10.1021/es2039695 | Environ. Sci. Technol. 2012, 46, 7018−7026

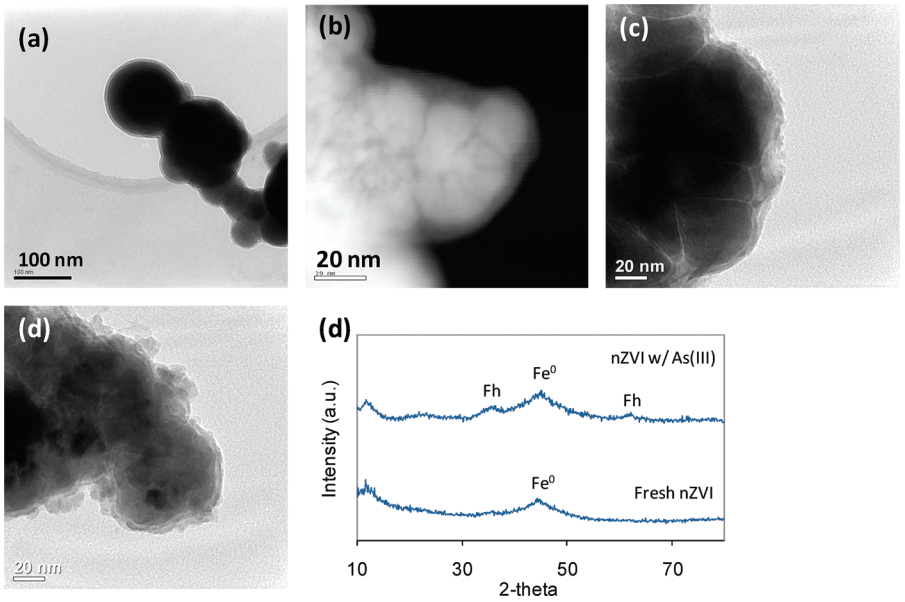

Figure 2. (a) TEM image of freshly made nZVI particles. (b) HAADF image of fresh nZVI showing a typical agglomerate consisting of a cluster of Fe(0) nuclei encapsulated by a continuous layer of iron oxide. (c) - (d) TEM images of nZVI reacted with As(III) for 24 h. (e) XRD patterns from the fresh and reacted nZVI materials. Fe^0 and Fh correspond to *bcc* Fe(0) and ferrihydrite, respectively.

Valence states of arsenic were analyzed using linear combination analysis (LCA) of the XANES spectra. Arsenic and iron EXAFS data were fit by nonlinear least-square methods using FEFF6 theory and the IFFEFIT software package.[33] Processing of the raw data was done by aligning the data in absolute energy, correcting for the pre-edge slope, normalizing by the edge step, and averaging to minimize the experimental errors for the steady-state regime. In previous studies, As(III) oxidation induced by X-ray irradiation was reported on powder samples.[12] The effect of X-ray irradiation on the As(III) solution used herein was estimated by taking repeated scans of a pure As(III) solution sample during 3 h of X-ray exposure. No appreciable change in the resultant spectra was observed (Figure S1, SI). We also evaluated X-ray irradiation effects on nZVI samples equilibrated with As(III). The spectra collected show no systematic changes that would suggest chemical changes due to beam exposure (Figure S2, SI).

The microstructure of nZVI before and after immersion in As(III) solution was characterized with bright field and high angle annular dark field (HAADF) transmission electron microscopy (TEM). Aqueous arsenic concentrations were determined using inductively coupled plasma-optical emission spectroscopy (ICP-OES). Details of the TEM characterization and aqueous sample analysis are available in the Supporting Information.

RESULTS

Characterization of nZVI. Analysis of the arsenic concentration in the solution phase indicates that nZVI at a mass loading above 1 g/L (Figure S3a, SI) sequestered more than 99% of the aqueous As(III) species. The rate of As(III) removal was considerably high. With 5 g/L nZVI, only 0.1% of the initial amount of aqueous As(III) remained in the solution 10 min after the onset of the experiment (Figure S1b, SI). These results establish that nearly all aqueous As(III) was captured by nZVI after the first 10 min, and the arsenic concentration in the solid phase was effectively constant during the ensuing period.

Figure 2a shows a transmission electron microscopy (TEM) image of freshly synthesized nZVI. The contrast between the electron-dense Fe(0) phase and the less-dense oxide material is evident in the high angle annular dark field (HAADF) image (Figure 2b), which shows a typical nZVI agglomerate comprised of a cluster of Fe(0) nuclei surrounded by a continuous oxide coating that was 2−10 nm in thickness. Independent XPS analysis of freshly made nZVI determined that the average thickness of this oxide layer was 2.4 nm, and high-resolution TEM characterization revealed a disordered structure.[31] The grain size of the Fe(0) core, estimated from its XRD pattern (Figure 2e) using the Scherrer equation, is ∼1 nm. For nZVI particles reacted with an aqueous As(III) solution for 24 h, there was no significant change in the core−shell configuration (Figure 2c-d and additional images in Figure S4, SI); however, the surface of the particles was decorated with loose debris of iron oxidation products, which corresponds to the growth of ferrihydrite shown in the XRD pattern (Figure 2e).

Arsenic Valence States in nZVI. To determine the valence states of arsenic in the reacted products, arsenic K-edge XANES spectra of reference arsenic compounds were collected, as shown in Figure 3. The As(V) spectrum was obtained from $Na_2HAsO_4{\cdot}7H_2O$ powder, but that of As(III) was measured using an aqueous solution of $NaAsO_2$ in order to minimize potential beam-induced As(III) oxidation that was observed previously.[12] Valence states of arsenic can be interpreted from the positions of absorption peaks in the XANES region. As shown in Figure 3, As(V) and As(III) exhibit absorption maxima at 11874.2 and 11870.7 eV, respectively. The energy shift of 3.5 eV between the two states is consistent with values reported in previous studies.[34,35] In addition, Figure 3 shows the elemental arsenic and arsenopyrite (FeAsS) data reported by Langner et al.[6] These XANES data were obtained at a bending magnet beamline with the same energy resolution by using the same Si(111) monochromator as in our work, thus it

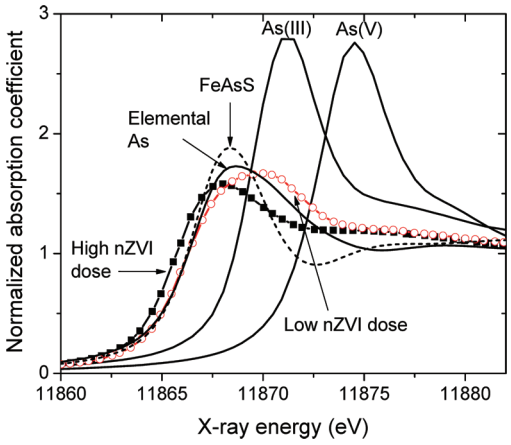

Figure 3. Arsenic K-edge XANES spectra of elemental arsenic (As(0)), arsenopyrite (FeAsS), As(III), and As(V) reference compounds and the products of As(III) (1.33 mM) reacted with a low (2 g/L) and high dose (5 g/L) of nZVI. Spectra of FeAsS and elemental arsenic are from Langner et al.[6]

is directly comparable with the data presented here. Furthermore, the X-ray energy scales of these spectra were aligned with our data by matching the peak positions of the As(III) compound from Langner et al.[6] with our As(III) reference.

In Figure 3 we provide the arsenic K-edge XANES spectra of the products of As(III) reacted with 2 g/L nZVI (denoted as a "low nZVI dose") and 5 g/L nZVI ("high nZVI dose") for 12 and 22 h, respectively. Time-dependent XANES data, discussed in the next section, suggests that arsenic transformations reached a quasi-steady state within the above time frames. The main absorption peak of the high nZVI dose sample appeared at a lower energy than those of elemental arsenic and FeAsS. Thus, the high dose experiment resulted in arsenic with an anionic character. This notion is supported by the lowering of the white line intensity of the high nZVI dose sample compared to the FeAsS and elemental arsenic data. A similar trend was noted in the data from Grosvenor et al.[28] showing that an increased anionic character of As with decreased concentration of P in $FeAs_xP_y$ compounds corresponds to a reduction of the white line in the arsenic K-edge XANES spectra. Since the valence state of arsenic in FeAsS is −1,[29] we propose the valence state for arsenic in the high nZVI dose sample to be −1 or lower. We note that this is likely a more accurate assignment than the previous notation of As(0), which was based on XPS analysis of the binding energy shift between the reduced arsenic and As(III).[25,26] The similarity between the local electronic and atomic environments around arsenic in our sample and FeAsS is also seen in the EXAFS data, as described further below.

In comparison to this high dose sample, arsenic captured using a low dose of nZVI showed an absorption maximum at 1.7 eV higher energy. The chemical nature of these states was further analyzed by using EXAFS.

Time-Dependent XANES Spectra. Dynamic transformation of arsenic in the presence of a low dose of nZVI was directly monitored by collecting time-dependent XANES spectra of the mixture in the reaction cell. Because of the rapid removal of aqueous As(III) by nZVI observed in the solution phase analysis, the spectra collected 5 min after the initiation of the experiment reflect primarily the process of arsenic transformation at the surface of nZVI. The time stamp of each spectrum represents the start time of an XANES scan. The scan frequency was approximately 5 min per scan during the first one-half hour and 14 min after that. The resultant data series shows distinct regimes during two time periods, the first one spanning 5 to 141 min (Figure 4) and the second one

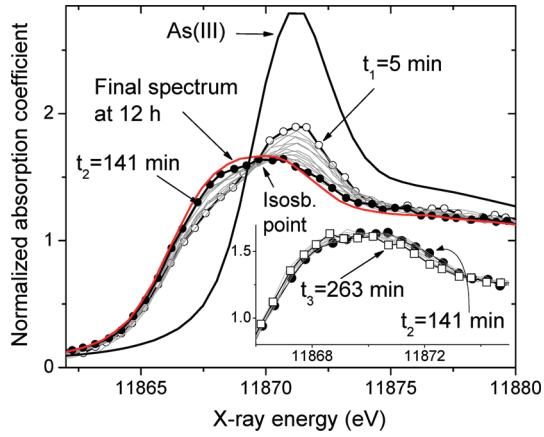

Figure 4. Time-resolved XANES spectra at the arsenic K-edge for the low nZVI dose experiment (1.33 mM As(III), 2 g/L nZVI). Overlay of the spectra collected during 5 to 141 min features an isosbestic point indicative of a two-phase arsenic transformation during this first time range. Inset: Overlay of the spectra collected during a second regime (≥141 min). In this time period a stable product was reached at 263 min and is characterized by a progressive translation of the curves to lower energies, which indicates structural transformations different from the isosbestic change in the first time period.

starting thereafter (Figure 4, inset). During the first period, the presence of an isosbestic point, i.e., an energy value where all spectra intersect each other, is evident. This feature indicates that during the first period there is a two-phase transformation in which the starting (As(III)) species progressively transform into an intermediate state. The presence of an intermediate state is also supported by principal component analysis (PCA) of the entire series of spectra. This method shows that the third principal component is distinctly above the noise level (Figure S5, SI), which corresponds to an intermediate state that is spectroscopically different from the starting and final states.[36,37]

Compared to the spectrum of an As(III) aqueous solution, the first spectrum collected at 5 min shows a pronounced decrease in the absorption maximum indicative of rapid transfer of free As(III) ions to the solid phase.[35] There is also a significant fraction of the arsenic intermediate species formed by this time as evidenced by the peak broadening to lower energy. Using the spectra at 5 and 141 min as references, the fraction of arsenic converted at intermediate times relative to the first time point (5 min) can be found using linear combination analysis (LCA). In this method, the first and last spectra within this time range are linearly combined to fit the intermediate data sets, where the mixing fraction is varied to achieve the best fit. An example of such analysis is presented in Figure S6a (SI). The high quality of the fit indicates this stage is dominated by a simple conversion from the initial state, i.e., adsorbed surface-bound As(III), to an intermediate state. Other spectra from the first regime were fit using the same procedure, and the results are plotted in Figure S6b (SI). In accordance with classic behavior giving rise to an isosbestic point, the curve exhibits first-order kinetics, where the half-life ($t_{1/2}$) of conversion was estimated to be 40 min. This rate of transformation is deemed more accurate compared to results

dx.doi.org/10.1021/es2039695 | Environ. Sci. Technol. 2012, 46, 7018−7026

Table 1. Best Fit Values for Coordination Numbers (N), Bond Lengths (R), and Their Mean Square Disorder Values (σ^2) for a Fresh nZVI Sample, As(V) Reference Compound, and As(III)-Treated nZVI Samples

sample	energy	coordination type	N	R (Å)	σ^2 (Å^2)
fresh nZVI	Fe K-edge	Fe−Fe	2.8 ± 0.8	2.42 ± 0.02	0.009 ± 0.003
As(V)	As K-edge	As−O	4 (fixed)	1.69 ± 0.04	0.003 ± 0.001
As(III) with high nZVI dose	As K-edge	As−O	-	-	-
		As−Fe	2.8 ± 0.5	2.42 ± 0.01	0.009 ± 0.001
As(III) with low nZVI dose	As K-edge	As−O	0.9 ± 0.7	1.78 ± 0.04	0.006 ± 0.012
		As−Fe	3.2 ± 1.6	2.50 ± 0.03	0.014 ± 0.005

we obtained previously using XPS, in which a limited number of time-dependent XPS data sets indicated that reduction of As(III) occurred on a time scale of hours.[25]

During the second stage (≥141 min), the spectra exhibited little change in the white line maxima. Instead, there was a gradual but noticeable shift of the curves to lower energies (Figure 4, inset) without isosbestic points. Comparing this series of spectra with the final spectrum at 12 h in Figure 3 indicates that stable products were established by 263 min. There were no appreciable changes in the spectra beyond this time.

Iron EXAFS Analysis. EXAFS analysis of a fresh nZVI sample found that iron in the nanoparticles was considerably more disordered than in a reference iron foil sample. The Fourier transform of the iron K-edge EXAFS data of the reference sample was identical to that of *bcc* iron (Figure S7). In comparison, the first (and only) coordination shell of iron in the fresh nZVI sample appears to be at a shorter distance with a much reduced coordination number. Atomic coordinates of *bcc* iron were used in the FEFF6 program to generate a theoretical EXAFS signal in order to fit the experimental data. The detailed bonding environment was determined by minimizing the residuals between the experimental data and the theoretical EXAFS spectrum, in which the following variables were adjusted to get the best fit: the coordination number (N), the average bond length (R), and the relative mean square displacement (σ^2, the EXAFS Debye−Waller factor) of the nearest neighboring shell. The EXAFS data of nZVI is best fit with an Fe−Fe coordination number (N) of 2.8 ± 0.8 and a bond length (R) of 2.42 Å (Table 1). The absence of higher order shells and the small coordination number (compared to the bulk value of 8) both appear to be caused by the strongly disordered and low dimensional metal core. This is consistent with XRD measurements showing that the core consists of crystallites of ∼1 nm in diameter. At this size scale, values of reduced N and smaller R compared to bulk materials are expected due to structural distortions[38,39] and surface relaxation induced by adsorbed ligands and impurities.[40] However, we cannot rule out the possibility of an amorphous-like iron phase being present in addition to polycrystalline *bcc* iron. For iron nanoparticles prepared by the borohydride reduction method, it has been noted that residual boron may form a glassy Fe−B phase.[41] In addition, EXAFS data of amorphous iron reported in previous studies show characteristics similar to our nZVI data including a reduction in the Fe−Fe bond length and the coordination number.[42,43] Therefore, it is difficult to distinguish the nature of polycrystalline and amorphous iron based on the available data here. Lastly, the absence of obvious Fe−O contributions in the EXAFS data may be interpreted as either structural disorder in the oxide shell, in accordance with electron microscopy observations, or the fraction of the oxide being relatively small, below the detection limit of XAS analysis (<10% in the present case).

Arsenic EXAFS Analysis. Figure 5 shows the arsenic K-edge data of the reacted samples, which were k^3-weighted and

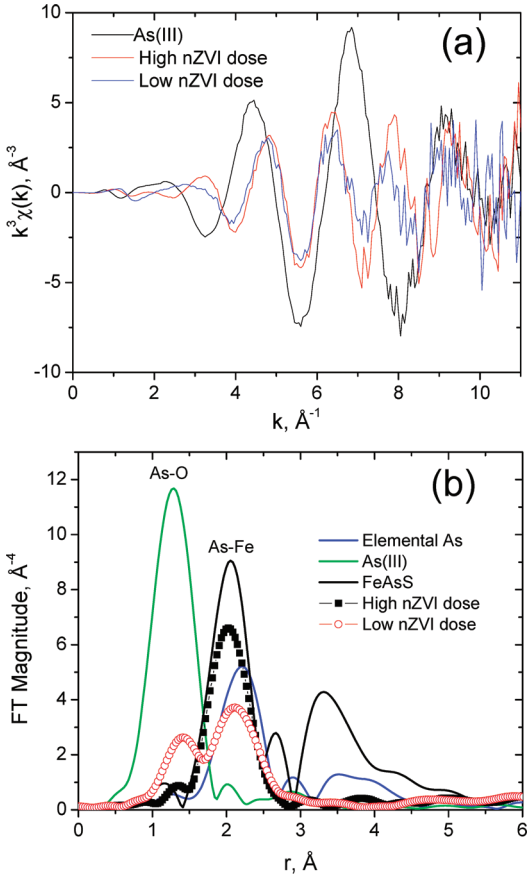

Figure 5. k^3-weighted EXAFS data for As(III) equilibrated with a low and high dose of nZVI (corresponding to the samples used in Figure 3) in (a) *k*-space and (b) *r*-space. Spectra of elemental As[6] and FeAsS[51] are shown for comparison. The low *r*-peak in (b) is due to As−O bonds and the high r-peak is due to As−Fe contributions, as demonstrated by comparing with the spectrum of FeAsS and the quantitative data analysis shown in Table 1. The absence of a higher *r* signal in both samples indicates a highly disordered structure beyond the first two coordination spheres of arsenic.

Fourier transformed using a Hanning window function in the *k*-range from 2 to 11 Å^{-1} at the arsenic K-edge. Reference elemental arsenic and FeAsS data transformed in the same conditions are shown in Figure 5 b for direct comparison.

Fitting of EXAFS data was done by constructing a theoretical FEFF6 model for two contributions, As−O and As−Fe. Our attempt to include an As−As contribution in the fitting was

dx.doi.org/10.1021/es2039695 | Environ. Sci. Technol. 2012, 46, 7018−7026

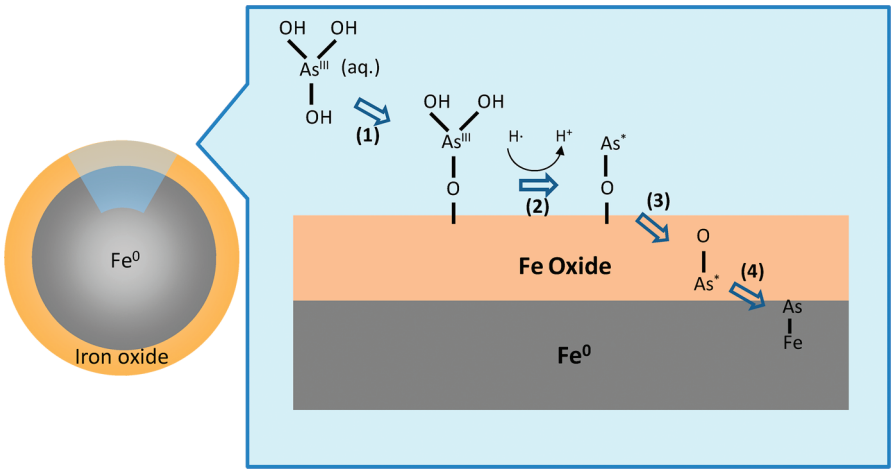

Figure 6. Proposed mechanism of As(III)-nZVI reactions. The process includes (1) rapid adsorption of aqueous As(III) at the oxide surface, (2) reduction of As(III) complexes at the surface, (3) translocation of arsenic across the oxide shell accompanied by further breaking of As−O bonds, and (4) diffusion into the Fe(0) core. Arsenic prefers to accumulate at the surface of Fe(0) forming a thin layer of Fe−As intermetallic, thus the amount of reduced arsenic depends on the amount of nZVI used. As* denotes intermediate states between As(III) and Fe−As intermetallic.

unsuccessful. The best fit results are shown in Figure S8 and Table 1. The passive electron reduction factor, S_0^2, was found to be 0.932 from the fit to an As(V) reference compound assuming the coordination number of As−O pairs was equal to four.[35,44] This S_0^2 value was fixed and used in the fits of the arsenic K-edge EXAFS data from the experimental samples. The results of EXAFS analysis indicate that the steady-state products of As(III) formed using the low and high doses of nZVI have different structures. In the presence of a high dose of nZVI, only one coordination shell of As−Fe bonding was identified, and there was no contribution from an As−O shell. This confirms that arsenic in this high dose sample was entirely converted to the reduced state. The As−Fe bond length of 2.42 Å measured in this sample is smaller than the distances in elemental arsenic (2.50 Å);[34] nevertheless, it agrees well with the Fe−Fe distance in fresh nZVI (Table 1). The value of N also matches with that of nZVI. The lack of high R structure suggests a disordered bonding environment, which is congruent with the nature of the Fe(0) phase deduced from the iron EXAFS analysis. Since no As−As bond was detected, formation of As(0) clusters embedded in the Fe(0) phase can be ruled out. These results allow us to postulate that arsenic and iron form an amorphous intermetallic phase.

Arsenic in the low dose nZVI sample can be satisfactorily fit with two coordination shells. The first shell at 1.78 Å corresponds to As−O coordination. This distance is in agreement with values reported in the literature for As(III) species.[34,35] The second shell is best fit by coordination to 3.2 iron atoms. The As−Fe bond length (2.50 Å) was slightly longer than that of the final arsenic species (2.42 Å) in the high dose sample but considerably smaller than the As−Fe distance in various iron oxide systems, such as ferrihydrite, goethite, and lepidocrocite (varying between 2.9 to 3.4 Å for bidentate mononuclear or binuclear configurations),[12,16] suggesting arsenic in this coordination shell interacts primarily with the Fe(0) component.

DISCUSSION

Implications for As(III) Sequestration Mechanisms. Prior investigations of As(III) sequestration with zerovalent iron by other researchers considered that As(III) was retained by ZVI materials mainly through surface adsorption[15,18] or via formation of arsenic−iron coprecipitates.[17,21] Reduction of As(III) was not observed in these previous studies, except that Bang et al. detected As(0) on an acid-treated iron coupon[20] and more recent work has identified As(0) underneath the surface oxide layer using XPS.[25,26] Thus, the lack of observation of arsenite reduction in previous studies may be due to the surface oxide layer acting as a barrier of electron transfer and material diffusion. It is also possible that reduced arsenic species are embedded underneath a growing ferrihydrite phase due to ongoing Fe(0) corrosion, making them inaccessible to XPS analysis or aqueous phase extraction. Therefore, XAS is the technique of choice to characterize solid-bound arsenic species within these nanoparticles.

XANES data presented herein show that, on a time scale of 22 h when using a high dose of nZVI (5 g/L), a predominant amount of As(III) was reduced to form an Fe−As intermetallic phase inside nZVI particles. There is no peak at a shorter distance (1.76−1.79 Å) corresponding to As−O bonds in As(III)-iron oxide surface complexes.[12,34] These observations are direct evidence that the reduced As is located in the metal phase of nZVI. Although the observed arsenic−iron intermetallic is rarely encountered in the natural environment, various forms of arsenic−iron compounds are found in many engineering materials. In ferromagnetic semiconductor systems, strong bonding between arsenic and iron is responsible for the formation of FeAs at the interface of an iron film deposited on a GaAs substrate.[45] Arsenic in these materials also exhibits preferential segregation on the surface of iron, which agrees with predictions based on theoretical calculations.[46,47] It is difficult to distinguish in our study whether arsenic atoms are enriched at the surface or diffused into the bulk Fe(0) phase because of the relatively large errors associated with N values in the best fit results (Table 1). However, consideration of similar systems described above would suggest arsenic enrichment at the surface of Fe(0) to be a more favorable configuration.

Quantitative EXAFS analysis results support visual observation (Figure 5b) that the local environment around arsenic in FeAsS is a reasonably good match to that of arsenic in the high nZVI dose sample. Arsenic in FeAsS is surrounded by 3 iron and 1 sulfur atoms, with As−Fe distances of 2.36−2.37 Å,[48]

dx.doi.org/10.1021/es2039695 | Environ. Sci. Technol. 2012, 46, 7018−7026

while the arsenic in the high dose sample is coordinated to 2.8 ± 0.5 iron atoms and the As−Fe distance is 2.42 ± 0.01 Å (Table 1). This implies that the sample bears a fair degree of structural similarity to FeAsS; however, the nature of our material (i.e., disorderliness and the absence of sulfur atoms) precludes us from proposing a more refined model.

With a smaller dose of nZVI (2 g/L), arsenic forms a partially reduced state between As(III) and the Fe−As intermetallic as reflected by the position of the absorption peak in the XANES spectrum. This is confirmed by the EXAFS data showing a shell of As−O coordination, which was absent in the high nZVI dose sample. The N value, despite its relatively large uncertainty, was significantly smaller than the theoretical value of three in a pure arsenite compound.[34,35] This indicates breaking of As−O bonds during the As(III) reduction process. The second shell of arsenic suggests As−Fe bonds at a distance slightly longer than the fully reduced arsenic species in the high dose sample, which may arise from increased disorder in the intermetallic phase as the arsenic content increases. On the basis of the fittings, we suggest that a mixture of arsenic states exists in this sample, a fraction of which interacts with the Fe(0) phase and the rest, constitutes of partially reduced arsenic species, coordinates with oxygen in the oxide phase.

Based on the EXAFS fitting and time-series XANES data from the low dose sample, we infer that the reduction process of As(III) consists of two stages of transformation. In the first stage (≤141 min), an isosbestic point in the spectra reflects decomposition of the original arsenic−iron-oxide surface complexes via breaking of As−O bonds, a process likely facilitated by nascent hydrogen produced by water reduction at the surface of the particles. In the second stage, which continued until a steady-state structure was obtained after 12 h, arsenic continued to lose oxygen (reduction) and migrated into the oxide film (diffusion). Arsenic diffusion is necessary to account for the bonding with metallic iron observed in the EXAFS data. Defects such as voids and structural misalignment in the amorphous oxide layer may provide channels for arsenic movement. The overall reaction mechanism is illustrated in Figure 6. We note that the end-point of arsenic transformation is affected by the amount of nZVI present, i.e., the ratio of iron to arsenic. At a high nZVI dose (5 g/L), the process ended with a complete loss of As−O bonds (below the XAS detection limit of 10%) and formation of a disordered Fe−As intermetallic phase. When a smaller amount of nZVI was present (2 g/L), a portion of the arsenic exists in a partially reduced state near the Fe(0)/oxide interface. The difference in the final states for different iron/arsenic ratios is an indication that arsenic may penetrate only a limited depth into the metal phase. Therefore, when a relatively large amount of arsenic is sequestered by nZVI, accumulation of arsenic species in the oxide phase close to the Fe(0) interface is expected. For nZVI particles of an average diameter of 60 nm (assuming the oxide thickness of ca. 2.4 nm is negligible compared to the diameter of the Fe(0) core), the dispersion number (D) of the nanoparticles, which is defined as the ratio of Fe(0) at the surface of the metal core to the total number of Fe(0) atoms,[49] is approximately 1.4×10^{-2} (details of this calculation in SI). If arsenic formed a monolayer at the Fe(0) core surface, we would expect the ratio of the reduced arsenic to Fe(0) in nZVI to be comparable to D. Experimentally, this ratio for the high dose sample was 1.9×10^{-2}. The reasonably good agreement between the two values supports our conclusion that arsenic tends to be enriched at the surface of the Fe(0) core and has limited mobility diffusing into the bulk of the core metal phase within the experimental time frame.

Importance of Complementary Investigations Using XPS and XAS. Prior *ex situ* investigations of As(III)-nZVI reactions with high-resolution XPS (HR-XPS) under similar solution conditions detected the presence of As(0), As(III), and As(V) in nZVI.[25] In addition, multiline XPS analysis using the widely spaced As3*d* and As2*p* signals revealed stratified distributions of different arsenic valence states within the near-surface region of the nanoparticles. Specifically, As(V) was found to exist primarily in the topmost surface layer on the oxide shell, As(III) was distributed throughout the oxide shell, and As(0) was embedded underneath the oxide layer at the core/shell interface.[26] Despite these insights gained by using XPS, it was difficult to quantify the amount of arsenic in different valence states due to their inhomogeneous distributions with depth. There is an intrinsic surface bias of XPS signals, because photoelectrons from near the surface experience less attenuation due to inelastic scattering and cause higher intensities than those from deeper regions.[30] Furthermore, the limited probe depth of XPS (~7 nm for As3*d* photoelectrons) precludes any information from the bulk solid phase.

Due to the high penetrating power of X-rays, with absorption lengths on the order of micrometers, XAS probes the entire nZVI particle. Furthermore, XAS can be performed under in situ conditions that are not available when using XPS or conventional extraction/dissolution analysis. Comparing results obtained with XPS and the present study at the same iron dose (5 g/L) and initial As(III) concentration (1.33 mM), we notice that a reduced arsenic state in an Fe−As intermetallic phase is the predominant species observed with XANES, while an As(0) peak constituted only 35% of the total arsenic signal in As3*d* XPS spectra. This highlights that As(III) can be nearly entirely reduced to an Fe−As intermetallic state in the presence of adequate nZVI. EXAFS analysis establishes that, at this iron dose, arsenic interacts with metallic iron only, which was inferred, but could not be unequivocally confirmed, by using XPS. Another notable difference is the detection of oxidized arsenic (As(V)) with XPS, which was not identified in the XANES analysis presented here. This is attributed in part to the inherent surface sensitivity of XPS analysis, which naturally tends to enhance signals of surface species such as As(V) that were found to form at the outer surface of the oxide shell.[26] However, drying of the samples necessitated by the UHV conditions required for XPS may alter the chemistry at the nZVI surface. Specifically, removal of the physically adsorbed water layer on the particles during drying may increase the local concentration of hydroxyl species and cause As(III) oxidation to be more favorable.[50]

■ ASSOCIATED CONTENT

Supporting Information

Detailed descriptions of the microscopy characterization and solution analysis procedures, calculations of the dispersion number of Fe(0) in nZVI, effect of X-ray irradiation on As(III) aqueous solutions (Figure S1) and on nZVI equilibrated with As(III) (Figure S2), solution analysis results (Figure S3), additional TEM micrographs of reacted nZVI (Figure S4), PCA analysis of time-series XANES spectra (Figure S5), LCA analysis (Figure S6), iron EXAFS data (Figure S7), and arsenic K-edge EXAFS best fit results (Figure S8). This material is available free of charge via the Internet at http://pubs.acs.org.

AUTHOR INFORMATION

Corresponding Author

*Phone: (609)258-4524. E-mail: bkoel@princeton.edu (B.E.K.). Phone: (212)340-7827. E-mail: anatoly.frenkel@yu.edu (A.I.F.).

Present Address

[⊥]Department of Civil and Environmental Engineering, Texas Tech University, Lubbock, TX 79409.

Notes

The authors declare no competing financial interest.

ACKNOWLEDGMENTS

Beamline X18B at the NSLS is supported in part by the Synchrotron Catalysis Consortium, U.S. Department of Energy Grant No DE-FG02-05ER15688. B.E.K. acknowledges support by the National Science Foundation under Grant No. CHE-1129417. A.I.F. and B.E.K. were supported in part by the Catalysis Center for Energy Innovation, an Energy Frontier Research Center funded by the U.S. Department of Energy, Office of Science, Office of Basic Energy Sciences, under award number DE-SC00010004. Synchrotron experiments were supported by U.S. Department of Energy Grant DE-FG02-03ER15476. The authors acknowledge A. A. Herzing and C. J. Kiely for providing the TEM images and P. Langner and G. Pokrovski for sharing their XANES and EXAFS data of elemental arsenic and arsenopyrite.

REFERENCES

(1) Smedley, P. L.; Kinniburgh, D. G. A review of the source, behaviour and distribution of arsenic in natural waters. *Appl. Geochem.* **2002**, *17* (5), 517−568.

(2) Korte, N. E.; Fernando, Q. A review of arsenic(III) in groundwater. *Crit. Rev. Environ. Control* **1991**, *21* (1), 1−39.

(3) Nordstrom, D. K. Public health - Worldwide occurrences of arsenic in ground water. *Science* **2002**, *296* (5576), 2143−2145.

(4) O'Day, P. A.; Vlassopoulos, D.; Root, R.; Rivera, N. The influence of sulfur and iron on dissolved arsenic concentrations in the shallow subsurface under changing redox conditions. *Proc. Natl. Acad. Sci. U.S.A.* **2004**, *101* (38), 13703−13708.

(5) Jones, C. A.; Langner, H. W.; Anderson, K.; McDermott, T. R.; Inskeep, W. P. Rates of microbially mediated arsenate reduction and solubilization. *Soil Sci. Soc. Am. J.* **2000**, *64* (2), 600−608.

(6) Langner, P.; Mikutta, C.; Kretzschmar, R. Arsenic sequestration by organic sulfur in peat. *Nat. Geosci.* **2012**, *5*, 66−73.

(7) Raven, K. P.; Jain, A.; Loeppert, R. H. Arsenite and arsenate adsorption on ferrihydrite: Kinetics, equilibrium, and adsorption envelopes. *Environ. Sci. Technol.* **1998**, *32* (3), 344−349.

(8) Dixit, S.; Hering, J. G. Comparison of arsenic(V) and arsenic(III) sorption onto iron oxide minerals: Implications for arsenic mobility. *Environ. Sci. Technol.* **2003**, *37* (18), 4182−4189.

(9) Goldberg, S.; Johnston, C. T. Mechanisms of arsenic adsorption on amorphous oxides evaluated using macroscopic measurements, vibrational spectroscopy, and surface complexation modeling. *J. Colloid Interface Sci.* **2001**, *234* (1), 204−216.

(10) Manceau, A. The mechanism of anion adsorption on iron oxides - Evidence for the bonding of arsenate tetrahedra on free Fe(O,OH) (6) edges. *Geochim. Cosmochim. Acta* **1995**, *59* (17), 3647−3653.

(11) Manning, B. A.; Fendorf, S. E.; Goldberg, S. Surface structures and stability of arsenic(III) on goethite: Spectroscopic evidence for inner-sphere complexes. *Environ. Sci. Technol.* **1998**, *32* (16), 2383−2388.

(12) Ona-Nguema, G.; Morin, G.; Juillot, F.; Calas, G.; Brown, G. E. EXAFS analysis of arsenite adsorption onto two-line ferrihydrite, hematite, goethite, and lepidocrocite. *Environ. Sci. Technol.* **2005**, *39* (23), 9147−9155.

(13) Sarkar, S.; Blaney, L. M.; Gupta, A.; Ghosh, D.; Sengupta, A. K. Arsenic removal from groundwater and its safe containment in a rural environment: Validation of a sustainable approach. *Environ. Sci. Technol.* **2008**, *42* (12), 4268−4273.

(14) Hussam, A.; Munir, A. K. M. A simple and effective arsenic filter based on composite iron matrix: Development and deployment studies for groundwater of Bangladesh. *J. Environ. Sci. Health, Part A: Toxic/Hazard. Subst. Environ. Eng.* **2007**, *42* (12), 1869−1878.

(15) Su, C. M.; Puls, R. W. Arsenate and arsenite removal by zerovalent iron: Kinetics, redox transformation, and implications for in situ groundwater remediation. *Environ. Sci. Technol.* **2001**, *35* (7), 1487−1492.

(16) Manning, B. A.; Hunt, M. L.; Amrhein, C.; Yarmoff, J. A. Arsenic(III) and Arsenic(V) reactions with zerovalent iron corrosion products. *Environ. Sci. Technol.* **2002**, *36* (24), 5455−5461.

(17) Nikolaidis, N. P.; Dobbs, G. M.; Lackovic, J. A. Arsenic removal by zero-valent iron: field, laboratory and modeling studies. *Water Res.* **2003**, *37* (6), 1417−1425.

(18) Kanel, S. R.; Manning, B.; Charlet, L.; Choi, H. Removal of arsenic(III) from groundwater by nanoscale zero-valent iron. *Environ. Sci. Technol.* **2005**, *39* (5), 1291−1298.

(19) Leupin, O. X.; Hug, S. J. Oxidation and removal of arsenic (III) from aerated groundwater by filtration through sand and zero-valent iron. *Water Res.* **2005**, *39* (9), 1729−1740.

(20) Bang, S.; Johnson, M. D.; Korfiatis, G. P.; Meng, X. G. Chemical reactions between arsenic and zero-valent iron in water. *Water Res.* **2005**, *39* (5), 763−770.

(21) Lien, H. L.; Wilkin, R. T. High-level arsenite removal from groundwater by zero-valent iron. *Chemosphere* **2005**, *59* (3), 377−386.

(22) Morin, G.; Wang, Y. H.; Ona-Nguema, G.; Juillot, F.; Calas, G.; Menguy, N.; Aubry, E.; Bargar, J. R.; Brown, G. E. EXAFS and HRTEM Evidence for As(III)-Containing Surface Precipitates on Nanocrystalline Magnetite: Implications for As Sequestration. *Langmuir* **2009**, *25* (16), 9119−9128.

(23) Hug, S. J.; Leupin, O. Iron-catalyzed oxidation of arsenic(III) by oxygen and by hydrogen peroxide: pH-dependent formation of oxidants in the Fenton reaction. *Environ. Sci. Technol.* **2003**, *37* (12), 2734−2742.

(24) Amstaetter, K.; Borch, T.; Larese-Casanova, P.; Kappler, A. Redox Transformation of Arsenic by Fe(II)-Activated Goethite (alpha-FeOOH). *Environ. Sci. Technol.* **2010**, *44* (1), 102−108.

(25) Ramos, M. A. V.; Yan, W.; Li, X. Q.; Koel, B. E.; Zhang, W. X. Simultaneous Oxidation and Reduction of Arsenic by Zero-Valent Iron Nanoparticles: Understanding the Significance of the Core-Shell Structure. *J. Phys. Chem. C* **2009**, *113* (33), 14591−14594.

(26) Yan, W. L.; Ramos, M. A. V.; Koel, B. E.; Zhang, W. X. Multi-tiered distributions of arsenic in iron nanoparticles: Observation of dual redox functionality enabled by a core-shell structure. *Chem. Commun.* **2010**, *46* (37), 6995−6997.

(27) O'Day, P. Chemistry and mineralogy of arsenic. *Elements* **2006**, *2* (2), 77−83.

(28) Grosvenor, A. P.; Cavell, R. G.; Mar, A. Bonding and Electronic Structure of Phosphides, Arsenides, and Antimonides by X-Ray Photoelectron and Absorption Spectroscopies. *Controlled Assem. Modif. Inorg. Syst.* **2009**, *133*, 41−92.

(29) Jones, R. A.; Nesbitt, H. W. XPS evidence for Fe and As oxidation states and electronic states in loellingite (FeAs2). *Am. Mineral.* **2002**, *87* (11−12), 1692−1698.

(30) *Practical Surface Analysis, Vol. 1: Auger and X-ray Photoelectron Spectroscopy*; Briggs, D., Seah, M. P., Eds.; John Wiley & Sons: New York, U.S., 1990.

(31) Martin, J. E.; Herzing, A. A.; Yan, W. L.; Li, X. Q.; Koel, B. E.; Kiely, C. J.; Zhang, W. X. Determination of the oxide layer thickness in core-shell zerovalent iron nanoparticles. *Langmuir* **2008**, *24* (8), 4329−4334.

(32) Sun, Y. P.; Li, X. Q.; Cao, J. S.; Zhang, W. X.; Wang, H. P. Characterization of zero-valent iron nanoparticles. *Adv. Colloid Interface Sci.* **2006**, *120* (1−3), 47−56.

(33) Newville, M.; Ravel, B.; Haskel, D.; Rehr, J. J.; Stern, E. A.; Yacoby, Y. Analysis of multiple-scattering XAFS data using theoretical standards. *Phys. B (Amsterdam, Neth.)* **1995**, *208* (1−4), 154−156.
(34) Foster, A. L.; Brown, G. E.; Tingle, T. N.; Parks, G. A. Quantitative arsenic speciation in mine tailings using X-ray absorption spectroscopy. *Am. Mineral.* **1998**, *83* (5−6), 553−568.
(35) Webb, S. M.; Gaillard, J. F.; Ma, L. Q.; Tu, C. XAS speciation of arsenic in a hyper-accumulating fern. *Environ. Sci. Technol.* **2003**, *37* (4), 754−760.
(36) Wang, Q.; Hanson, J. C.; Frenkel, A. I. Solving the structure of reaction intermediates by time-resolved synchrotron X-ray absorption spectroscopy. *J. Chem. Phys.* **2008**, *129*, 234502−7.
(37) Frenkel, A. I.; Kleifeld, O.; Wasserman, S.; Sagi, I. Phase speciation by extended X-ray absorption fine structure spectroscopy. *J. Chem. Phys.* **2002**, *116*, 9449.
(38) Gilbert, B.; Huang, F.; Zhang, H. Z.; Waychunas, G. A.; Banfield, J. F. Nanoparticles: Strained and stiff. *Science* **2004**, *305* (5684), 651−654.
(39) Thoral, S.; Rose, J.; Garnier, J. M.; Van Geen, A.; Refait, P.; Traverse, A.; Fonda, E.; Nahon, D.; Bottero, J. Y. XAS study of iron and arsenic speciation during Fe(II) oxidation in the presence of As(III). *Environ. Sci. Technol.* **2005**, *39* (24), 9478−9485.
(40) Yevick, A.; Frenkel, A. I. Effects of surface disorder on EXAFS modeling of metallic clusters. *Phys. Rev. B* **2010**, *81* (11), 7.
(41) Carpenter, E. E.; Calvin, S.; Stroud, R. M.; Harris, V. G. Passivated iron as core-shell nanoparticles. *Chem. Mater.* **2003**, *15* (17), 3245−3246.
(42) Long, G. J.; Hautot, D.; Pankhurst, Q. A.; Vandormael, D.; Grandjean, F.; Gaspard, J. P.; Briois, V.; Hyeon, T.; Suslick, K. S. Mossbauer-Bauer-effect and x-ray-absorption spectral study of sonochemically prepared amorphous iron. *Phys. Rev. B* **1998**, *57* (17), 10716−10722.
(43) Kataby, G.; Prozorov, T.; Koltypin, Y.; Cohen, H.; Sukenik, C. N.; Ulman, A.; Gedanken, A. Self-assembled monolayer coatings on amorphous iron and iron oxide nanoparticles: Thermal stability and chemical reactivity studies. *Langmuir* **1997**, *13* (23), 6151−6158.
(44) Kim, J.; Korshin, G. V.; Frenkel, A. I.; Velichenko, A. B. Electrochemical and XAES studies of effects of carbonate on the oxidation of arsenite. *Environ. Sci. Technol.* **2006**, *40* (1), 228−234.
(45) LeBeau, J. M.; Hu, Q. O.; Palmstrom, C. J.; Stemmer, S. Atomic structure of postgrowth annealed epitaxial Fe/(001) GaAs interfaces. *Appl. Phys. Lett.* **2008**, *93* (12), 121909.
(46) Schultz, B. D.; Farrell, H. H.; Evans, M. M. R.; Ludge, K.; Palmstrom, C. J. ErAs interlayers for limiting interfacial reactions in Fe/GaAs(100) heterostructures. *J. Vac. Sci. Technol., B: Microelectron. Nanometer Struct.--Process., Meas., Phenom.* **2002**, *20* (4), 1600−1608.
(47) Mirbt, S.; Sanyal, B.; Isheden, C.; Johansson, B. First-principles calculations of Fe on GaAs(100). *Phys. Rev. B* **2003**, *67* (15), 155421.
(48) Buerger, M. J. The symmetry and crystal structure of the minerals of the arsenopyrite group. *Z. Kristallogr.* **1936**, *95*, 83−113.
(49) Somorjai, G. A. *Introduction to Surface Chemistry and Catalysis*; John Wiley & Sons: New York, U.S., 1994; pp 6−12.
(50) Manning, B. A.; Goldberg, S. Adsorption and stability of arsenic(III) at the clay mineral-water interface. *Environ. Sci. Technol.* **1997**, *31* (7), 2005−2011.
(51) Borisova, A. Y.; Pokrovski, G. S.; Pichavant, M.; Freydier, R.; Candaudap, F. Arsenic enrichment in hydrous peraluminous melts: Insights from femtosecond laser ablation-inductively coupled plasma-quadrupole mass spectrometry, and in situ X-ray absorption fine structure spectroscopy. *Am. Mineral.* **2010**, *95* (7), 1095−1104.